Published in final edited form as:
Fluid Dyn Res. 2012 ; 44(5): 055503–. doi:10.1088/0169-5983/44/5/055503.

Elastic capsule deformation in general irrotational linear flows

Alex C. Szatmary and **Charles D. Eggleton**
Department of Mechanical Engineering, University of Maryland, Baltimore County, Baltimore, MD 21250, USA

Charles D. Eggleton: eggleton@umbc.edu

Abstract

Knowledge of the response of elastic capsules to imposed fluid flow is necessary for predicting deformation and motion of biological cells and synthetic capsules in microfluidic devices and in the microcirculation. Capsules have been studied in shear, planar extensional, and axisymmetric extensional flows. Here, the flow gradient matrix of a general irrotational linear flow is characterized by two parameters, its strain rate, defined as the maximum of the principal strain rates, and by a new term, q, the difference in the two lesser principal strain rates, scaled by the maximum principal strain rate; this characterization is valid for ellipsoids in irrotational linear flow, and it gives good results for spheres in general linear flows at low capillary numbers. We demonstrate that deformable non-spherical particles align with the principal axes of an imposed irrotational flow. Thus, it is most practical to model deformation of non-spherical particles already aligned with the flow, rather than considering each arbitrary orientation. Capsule deformation was modeled for a sphere, a prolate spheroid, and an oblate spheroid, subjected to combinations of uniaxial, biaxial, and planar extensional flows; modeling was performed using the immersed boundary method. The time response of each capsule to each flow was found, as were the steady-state deformation factor, mean strain energy, and surface area. For a given capillary number, planar flows led to more deformation than uniaxial or biaxial extensional flows. Capsule behavior in all cases was bounded by the response of capsules to uniaxial, biaxial, and planar extensional flow.

1. Introduction

It is important to model the behavior of capsules in a wide variety of flows, to predict their deformation and motion and to make comparisons with experiments to determine material properties. A red blood cell can be modeled as an elastic capsules, that is, a membrane both enclosing fluid and immersed in fluid. Elastic capsules can also be generated synthetically, (Rehage et al. 2002, Walter et al. 2001, Chang & Olbricht 1993*a*, Chang & Olbricht 1993*b*) with applications in drug delivery.

Previous studies have focused on the physics of capsules in uniaxial extensional flows and planar shear flows. Planar flows, such as shear and hyperbolic extensional flows, can be generated by a four roll mill and applied to elastic capsules (Walter et al. 2001, Chang & Olbricht 1993*a*, Chang & Olbricht 1993*b*); they also appear in channels with high aspect ratio cross-sections. It is convenient to model axisymmetric extensional flows computationally, because the symmetry of the problem reduces the number of dimensions that need to be modeled (Diaz et al. 2000). Capsules have been modeled extensively using the boundary element method (Diaz et al. 2000, Pozrikidis 1995, Barthès-Biesel et al. 2002, Diaz et al. 2001, Dodson & Dimitrakopoulos 2008, Dodson & Dimitrakopoulos 2009, Gupta et al. 2009) and the immersed boundary method (Bagchi & Kalluri 2009, Eggleton & Popel 1998, Doddi & Bagchi 2009, Bagchi et al. 2005, Sui et al. 2008, Shin & Sung 2011, Song et al. 2011), typically in shear or axisymmetric extensional flow. Capsule deformation has also been modeled in planar flows (Bagchi & Kalluri 2009, Eggleton & Popel 1998, Ramanujan

& Pozrikidis 1998) and in Poiseuille flows (Doddi & Bagchi 2009, Pappu et al. 2008). Perturbation analyses for small deformations have been performed (Barthès-Biesel & Rallison 1981, Barthès-Biesel 1980, Barthès-Biesel & Sgaier 1985, Barthès-Biesel & Chhim 1981). The physics of capsules is studied in idealized flows, but capsules are subjected to more general flows; study of capsule physics in non-planar, non-axisymmetric flow is necessary to obtain insight about the full scope of the deformation of capsules, to relate findings in ideal flows to behavior of capsules undergoing complex flows.

We characterize an irrotational linear flow by its intensity, the maximum principal strain rate, $\dot{\varepsilon}$, and a new term, q, the relative difference in the other two principal strain rates (q represents how two-dimensional a flow is). Red blood cells, bacteria, and many synthetic capsules are non-spherical, they have inherent orientation. Consequently, the response of non-spherical particles in flow fields would need to be determined for all particle orientations relative to the flow, unless the particles are prone to aligning with the flow. Jeffery (1922) found, analytically, how ellipsoidal particles move in linear viscous flow; Taylor (1923) experimentally confirmed these predictions. Jeffery's analysis predicts that rigid ellipsoids will align with irrotational flow. We show that deformable non-spherical elastic capsules align with the principal axes of irrotational flow. Rather than study the deformation of a non-spherical particle in every orientation, it is more practical to study capsule deformation with the capsule aligned with the flow field. For simplicity, this study is restricted to irrotational flow; this is a useful simplification because deformation is mostly due to the elongational component of the flow. Tank-treading, vacillating, and tumbling, as seen for ellipsoidal capsules in shear flow, e.g., in (Rehage et al. 2002, Walter et al. 2001, Bagchi & Kalluri 2009, Sui et al. 2008, Ramanujan & Pozrikidis 1998), require vorticity in the flow, and so these behaviors are not exhibited in the results presented here.

We present numerical results obtained using the immersed boundary method (Peskin 1977) for spherical and spheroidal capsules in linear combinations of uniaxial extensional flow and planar extensional flow, and biaxial extensional flow and planar extensional flow. This yields the deformation physics for the capsules considered here in all irrotational linear flows; this also gives good results for spherical capsules in general linear flow at low capillary numbers. To our knowledge, this is the first study of elastic capsules in a biaxial extensional flow, as well as the first study of elastic capsules in flows that are superpositions of planar and axisymmetric flows. In addition, this perspective—looking at capsule physics in general irrotational linear flow—gives insight about capsule deformation in the specific cases of planar flows (e.g., shear flow) and axisymmetric flows.

2. Defining linear flows on capsules

The physics of capsules in unbounded flow has been studied for planar and axisymmetric flows. In this section, the deformation of capsules is discussed for a broader category, linear flows. A measure of flow gradient intensity is presented, allowing comparison of capsule deformation under a variety of flows. The flow gradient matrix is reduced so that all deformations under irrotational linear flow can be generated by the variation of two parameters.

To simplify the problem, the capsule membrane material is assumed to be elastic, uniform, isotropic, and of negligible thickness. Also, the flow is assumed to be in the Stokes regime. The fluid and membrane physics are mediated by the no-slip condition and membrane impermeability, and the dynamic equilibrium of the membrane. It is assumed that the fluid enclosed by the capsule has the same properties as the external fluid.

For the linear flow field,

$$\mathbf{u}=\mathbf{u}|_{\mathbf{x}=0}+\mathbf{E}\cdot\mathbf{x}, \quad (1)$$

the fluid velocity, **u** can be represented by twelve terms, three for the mean flow and nine for the flow gradient; if only the physics of the capsule are to be considered, many of these variables are redundant. For example, deformation is not a function of the mean flow, **u**, this mean flow only leads to translation, so it is ignored.

For irrotational flows, the flow gradient matrix, **E** is symmetric. The induced 2-norm is appropriate for characterizing **E** because it is the norm that is constant under coordinate system rotation. Here, the characteristic strain rate $\dot{\varepsilon}$, is defined to be the 2-norm of **E**; $\dot{\varepsilon}$ is the maximum of the absolute values of the principal strain rates. Eigen decomposition gives the principal strain rates of **E**, its eigenvalues, $\dot{\varepsilon}_1$, $\dot{\varepsilon}_2$, and $\dot{\varepsilon}_3$, sorted such that $|\dot{\varepsilon}_1| \geq |\dot{\varepsilon}_2| \geq |\dot{\varepsilon}_3|$. Because the flow is incompressible, the trace of the matrix is zero, $\dot{\varepsilon}_1 + \dot{\varepsilon}_2 + \dot{\varepsilon}_3 = 0$. For irrotational flow, capsule deformation is a function only of the principal strain rates of **E**, so equivalent capsule deformation can be generated by a diagonal matrix, **D**; the values on the diagonal are the principal strain rates $\dot{\varepsilon}_1$, $\dot{\varepsilon}_2$, and $\dot{\varepsilon}_3$.

The relative difference between the lesser two principal strain rates,

$$q=\frac{\dot{\varepsilon}_3-\dot{\varepsilon}_2}{\dot{\varepsilon}_1}, \quad (2)$$

emerges as a second characteristic of the flow gradient matrix. Given the sorting of the eigenvalues, q can vary from 0 to 1. The matrix, **E**, can be posed in terms of $\dot{\varepsilon}_1$ and q,

$$\mathbf{D}=\begin{bmatrix}\dot{\varepsilon}_1 & & \\ & \dot{\varepsilon}_2 & \\ & & \dot{\varepsilon}_3\end{bmatrix}=\dot{\varepsilon}_1\begin{bmatrix}1 & & \\ & \dot{\varepsilon}_2/\dot{\varepsilon}_1 & \\ & & \dot{\varepsilon}_3/\dot{\varepsilon}_1\end{bmatrix}=\dot{\varepsilon}_1\begin{bmatrix}1 & & \\ & -(1+q)/2 & \\ & & -(1-q)/2\end{bmatrix}. \quad (3)$$

Varying $\dot{\varepsilon}_1$ over all real numbers, and varying q from 0 to 1, can be used to generate any capsule deformation that could be generated under irrotational linear flow. The maximum principal strain rate, $\dot{\varepsilon}_1$, can be either positive or negative, so the flow can be primarily extensional (positive) or compressive (negative). The characteristic strain rate, $\dot{\varepsilon}$, is the absolute value of $\dot{\varepsilon}_1$; this leads to the definition of two types of flow gradient matrix,

$$\mathbf{E}_{up}(\dot{\varepsilon},q)=\dot{\varepsilon}\begin{bmatrix}1 & & \\ & -(1+q)/2 & \\ & & -(1-q)/2\end{bmatrix}, \quad (4)$$

$$\mathbf{E}_{bp}(\dot{\varepsilon},q)=\dot{\varepsilon}\begin{bmatrix}-1 & & \\ & (1+q)/2 & \\ & & (1-q)/2\end{bmatrix}. \quad (5)$$

Two **E** matrices are needed to model capsule deformation under all irrotational linear flows, because $\dot{\varepsilon}$ is held positive. The matrix $\mathbf{E}_{up}(\dot{\varepsilon}, q)$ corresponds to uniaxial extensional flow at $q = 0$,

$$\mathbf{u}_u=\dot{\varepsilon}\,(x,-y/2,-z/2), \quad (6)$$

and planar extensional flow at $q = 1$,

$$\mathbf{u}_p = \dot{\varepsilon}\,(x, -y, 0). \quad (7)$$

Similarly, the matrix $\mathbf{E}_{bp}(\dot{\varepsilon}, q)$ corresponds to biaxial extensional flow at $q = 0$,

$$\mathbf{u}_b = \dot{\varepsilon}\,(-x, y/2, z/2), \quad (8)$$

and planar extensional flow (7) at $q = 1$. Here, uniaxial flow has one axis of extension and two of compression; biaxial flow has two axes of extension and one of compression.

This characterization of $\mathbf{E}$ by $\dot{\varepsilon}$ and q is apt for a deformable particle in any irrotational flow, provided that the flow is viscous and that the particle is aligned with the principal axes of the flow. Rigid body rotation causes negligible deformation of spherical capsules at low capillary numbers (Barthès-Biesel & Rallison 1981), so this characterization is also appropriate for spherical capsules in any low capillary number linear flow, regardless of the vortical component of the flow.

3. Computational model

3.1. Numerical method

It is assumed that the fluid is incompressible and Newtonian. In this work, flows are considered at sufficiently low Reynolds numbers that viscous forces dominate, so the convective terms can be ignored. The unsteady Stokes equation,

$$\rho\frac{\partial \mathbf{u}}{\partial t} + \nabla p = \mu\nabla^2\mathbf{u} + \mathbf{F}(\mathbf{x}), \quad (9)$$

is solved by Chorin's (1968) projection method, implemented as in (Peskin 1977), but with a divergence operator presented in (Peskin & Printz 1993) to provide improved volume conservation. The fluid is discretized as a uniform cubic grid. Here, $\mathbf{F}(\mathbf{x})$ represents forces applied to the fluid from the immersed structure. The flow field is also subject to the continuity equation,

$$\nabla \cdot \mathbf{u} = 0. \quad (10)$$

The immersed boundary method was used to model the fluid-structure interaction in this problem (Peskin 1977), based on the implementation in (Eggleton & Popel 1998). The capsule is modeled on a Lagrangian mesh, and the fluid is modeled on an Eulerian grid. A discrete approximation of the Dirac delta,

$$\delta_h(\mathbf{x}) = d_h(x_1/h)\,d_h(x_2/h)\,d_h(x_3/h) \quad (11)$$

is used, where h is the fluid grid spacing; d_h, the corresponding one-dimensional discrete Dirac delta, is defined as

$$d_h(r)=\begin{cases}\frac{3-2|r|+\sqrt{1+4|r|-4r^2}}{8}, & |r|\le 1,\\ \frac{5-2|r|-\sqrt{-7+12|r|-4r^2}}{8}, & 1\le|r|\le 2,\\ 0 & 2\le|r|.\end{cases} \quad (12)$$

The force exerted by the capsule mesh, **f**, is converted into the **F** in the fluid coordinate system by,

$$\mathbf{F}_{i,j,k}=\sum_m \mathbf{f}_m \delta_h(\mathbf{x}_{i,j,k}-\mathbf{X}_m), \quad (13)$$

where $\mathbf{X}_m$ is the coordinate of the m-th node in the discretized capsule, and is the coordinate of a fluid node. This spreads the force from a single capsule node onto the fluid nodes in its neighborhood, two nodes in each direction. Likewise, the velocities of the capsule nodes are found by interpolating from the velocities on the nearby fluid nodes, $\mathbf{x}_{i,j,k}$,

$$\mathbf{U}_m=\sum_{i,j,k}\mathbf{u}_{i,j,k}\delta_h(\mathbf{x}_{i,j,k}-\mathbf{X}_m), \quad (14)$$

where $\mathbf{U}_m$ is the velocity of material node $\mathbf{X}_m$. The new positions of the material nodes are then given by displacing them using the fluid velocity interpolated onto the elastic mesh,

$$\mathbf{X}^{n+1}=\mathbf{X}^n+\Delta t\mathbf{U}^{n+1}(\mathbf{X}^n,t), \quad (15)$$

completing the time step.

3.2. Model set-up

In all computations here, the capsule was modeled as fluid enclosed by a neo-Hookean membrane, with a strain energy function given by

$$W=\frac{Eh}{6}\left(\lambda_1^2+\lambda_2^2+\lambda_1^{-2}\lambda_2^{-2}-3\right), \quad (16)$$

where Eh is the membrane stiffness, with E three times the shear modulus G; λ_1 and λ_2 are the major and minor stretch ratios. This analysis could be applied to other membrane constitutive equations; the neo-Hookean model is used here for simplicity as only one material property is invoked. The capsule is discretized as a mesh of 81,920 triangular elements. Stretch ratios are calculated for each element. The forces exerted on each node by each element are found by taking the derivative of the strain energies with respect to the stretch ratios and applying the forces along the principal strain axes (Oden 1972). Three capsules were modeled, a sphere, a prolate spheroid, and an oblate spheroid. The prolate spheroid has an aspect ratio of 2:1:1, while the oblate spheroid has an aspect ratio of 2:2:1. The spheroids have similar proportions, just different axes of symmetry. They are scaled to have the same surface area as the sphere.

Each capsule was subjected to the flows described by (4) and (5), for q = 0, 0.1, 0.2,…, 1. The characteristic strain rate of the fluid is represented non-dimensionally as the capillary number,

$$Ca = \frac{a\,\dot{\varepsilon}\,\mu}{Eh}, \quad (17)$$

where a is the characteristic length of the capsule and μ is the viscosity. Under this scheme, the characteristic time is $1/\dot{\varepsilon}$. The time step was adjusted with the capillary number, so that non-dimensional time units were modeled. For stability, the timestep used was $0.05Ca$. For a sphere, the characteristic length is its radius. Ellipsoids are considered here, also; we define the characteristic length of an ellipsoid to be the radius of a sphere of the same surface area, $a = \sqrt{A/4\pi}$, where A is the surface area of the ellipsoid, as in (Kraus et al. 1996).

Simulations were performed for capillary numbers of 0.01, 0.02, and 0.04; unless otherwise stated, the data shown is for a capillary number of 0.04. The ratio of the width of the computational domain to the radius of the capsule was 12; deviation in results for this domain and for tests on an equivalent domain of half this size were less than 3%. The fluid domain was discretized as a uniform cubic lattice, with 64 nodes in each coordinate direction, for a total of $64^3 = 262,144$ nodes.

4. Results

4.1. Ellipsoids align with irrotational flow fields

The elongational component of the flow can be expressed by $\dot{\varepsilon}$ and q; this exploits the symmetry of spheres by conveniently re-orienting the coordinate system. To characterize flow on a non-spherical particle, every orientation of the particle would need to be considered; this would be unwieldy. The problem of finding the steady-state deformation of the particles is simplified if the capsules tend to align with the principal axes of the flow. It is already well-known that rigid ellipsoids align with irrotational viscous linear flows (Jeffery 1922). To demonstrate that deformable ellipsoids align with irrotational flow, orientation of prolate and oblate spheroids was modeled in uniaxial, biaxial, and planar extensional flows.

The orientation of the spheroidal capsules is described by the spherical coordinates φ and θ. Figure 1 shows a prolate spheroid in this coordinate system. The direction of axisymmetry of this spheroid is $\hat{n}$. The free-stream principal strain rate with the highest magnitude is on the x-axis, and the minimum is on the z-axis, so for the uniaxial and biaxial extensional flows, the x-axis is the direction of axisymmetry for the flow. For axisymmetric flows, $\varphi = \pi/2$ corresponds to the axes of the capsule and the flow being identical, while $\varphi = 0$ corresponds to the axes of the capsule and the flow being perpendicular. For planar extensional flows, extension occurs in the x-direction and compression in the y. The elevation of $\hat{n}$ from the $y - z$ plane is φ; θ is the azimuthal angle from the $x - y$ plane. In this case, $\varphi = \pi/2$ is the direction of elongation, $\varphi = 0$ and $\theta = 0$ is the direction of compression, and $\varphi = 0$ and $\theta = \pi/2$ is the out-of-plane direction. The alignment of prolate and oblate spheroids in uniaxial, biaxial, and planar extensional flows was computed for a variety of initial orientations. For all cases, φ was varied. The azimuthal angle, θ, was also varied for the planar case; θ is redundant for the axisymmetric flows.

The angle, φ, between the major axis of a prolate capsule and the $y - z$ plane of a uniaxial extensional flow is shown in Figure 2. In all cases, the capsule's orientation changes so that the major axis aligns with the direction of elongation, the x-axis ($\varphi = \pi/2$). For $\varphi_0 = 0$, the axis of symmetry of the spheroid was originally perpendicular to that of the flow. In this case, the capsule's orientation is initially at an unstable fixed point; a slight perturbation in its orientation destabilizes it. This perturbation would arise in nature from, say, slight initial deviation of the capsule's axis from $\varphi = 0$, or from thermal fluctuations. In this model, we

place the capsule slightly off-axis to produce this instability. The capsule gradually departs from the $\varphi = 0$ state, then settles at $\varphi = \pi/2$, at which point its major axis is aligned with the extensional component of the flow. The case with $\varphi_0 = \pi/4$ skips the initial destabilization step and displays a similar settling behavior. The case in which the capsule is initially aligned with the flow field ($\varphi_0 = \pi/2$) was also modeled; the capsule did not rotate from this resting position. For different combinations of capsule shape, prolate or oblate, and flow field, uniaxial, biaxial, or planar extensional, the effect of varying the initial φ is similar: regardless of the initial φ, for a given capsule and flow field, all cases will lead to the same steady-state orientation.

The evolution of the angle, φ, between the major axis of a spheroid and the $y - z$ plane is shown in Figure 3 for each combination of uniaxial, biaxial, and planar extensional flows, with both prolate and oblate spheroidal geometries. The initial orientation of each capsule was picked to be perpendicular to its resting orientation. In each case, the major axis of an ellipsoid aligns with extension and the minor axis aligns with compression.

The profile of an oblate capsule in a biaxial extensional flow (8) is shown for several different timesteps in Figure 4. Initially, the axis of symmetry of the spheroid, the short axis, is aligned with the flow. The capsule quickly deforms under the flow, but, as is clear at $t = 15$, there are bulges on the sides of the deformed shape, corresponding to the edge of the spheroid at rest. On a longer timescale, the flow causes this edge, the widest part of the reference shape, to move to align with the direction of extension in the flow. These two timescales are evident in Figure 3, in which the capsules orient first slowly, then quickly.

For the simulation results shown in Figure 3, capsules in planar extensional flow were only oriented in plane with the flow. To explore the alignment with planar flow of capsules initially oriented out-of-plane, a prolate capsule was positioned in-plane ($\theta = 0$) and out of plane at $\theta = \pi/4$ and $\theta = \pi/2$, with an initial φ of 0; this is shown in Figure 5. In each case, the capsule's major axis converged to the direction of maximum extensional strain rate, $\varphi = \pi/2$.

An oblate capsule was positioned at azimuthal angles, θ, of 0, $\pi/4$, and $\pi/2$. In all cases, the semi-minor axis converged to the direction of maximum compressive strain rate ($\theta = 0$), as shown in Figure 6. This consideration of capsules initially oriented out of the plane of flow shows that both the major and minor axes align with the flow.

In irrotational linear flows, ellipsoidal capsules align with the flow such that the longest axis coincides with the greatest extension in the flow, while the shortest axis coincides with the greatest compression. These results agree with the predictions of Jeffery's (1922) for rigid ellipsoids. We modeled capsules at a capillary number of 0.04 and saw that they aligned with the imposed flow; capsules will certainly align with flow at lower capillary numbers, corresponding to stiffer membranes. Because this alignment occurs, the initial orientation of an ellipsoidal capsule does not affect the steady-state deformation of the capsule. Therefore, the effects of irrotational linear flow on a non-spherical capsule at steady-state can be expressed as a function of just Ca and q, just as for a sphere.

4.2. Capsule deformation in irrotational linear flow

The deformation physics of capsules under combinations of planar and uniaxial extensional flows (4) and planar and biaxial extensional flows (5) were determined computationally. These flows are characterized by q, the relative difference in the lesser principal strain rates (2). At $q = 0$, depending on the case, the flow is perfectly uniaxial (6) or biaxial (8); at $q = 1$, the flow is a planar extensional flow (7). Three capsules were considered, a sphere, a prolate

spheroid, and an oblate spheroid. A non-dimensional shear rate of $Ca = 0.04$ was applied to the capsules.

The shape deformations of the capsules were characterized by

$$D=\frac{a(t)/A-b(t)/B}{a(t)/A+b(t)/B}, \quad (18)$$

where $a(t)$ and $b(t)$ are the semi-major and semi-minor axes of the capsule as functions of time, and A and B are the semi-major and semi-minor axes of the capsule at rest, as in (Diaz et al. 2000); for the sphere, this gives the Taylor deformation factor. The deformation, D, is shown in Figure 7 for each of the capsules, in uniaxial-planar and biaxial-planar flow fields. The oblate spheroid was much less sensitive to q than the sphere and prolate spheroid. Capsule deformation under imposed flow can be used to infer membrane stiffness by comparing with a model for deformation versus stiffness (Chang & Olbricht 1993*b*). Of course, uncertainty about the strain rate of the flow field leads to uncertainty about the stiffness; these results show that uncertainty about the type of the flow field contributes to considerable uncertainty about the membrane stiffness. When interpreting measurements made in a four-roll mill, for example, it is assumed that the flow is planar, $q = 1$. If end effects were significant, though, the actual q would not be 1, altering the estimate of the membrane stiffness.

Figure 8 shows the increase in the surface area of the capsule subjected to flow, as a percentage of the unstressed surface area. The application of flow leads to an increased surface area in all cases, up to an 18% increase. For each capsule, the surface area varies only slightly with q for biaxial-planar flows, but increases with q for the uniaxial-planar case.

The time evolution of D is shown in Figure 9 for selected flows. Each trend is similar, in the form of an exponential settling. The evolution of D is fitted to a curve of the form,

$$D^*(t)=D_\infty \times (1-\exp(1-t/\tau)), \quad (19)$$

where D_∞ is the steady-state D, as in (Diaz et al. 2000). The response time, τ, for a given Ca and q was inferred from this fit; it is shown in Figure 10 for each flow considered. Under uniaxial-planar flows, the response time of the sphere and prolate spheroid was slightly non-monotonic with q, but the maximum value is above the τ for planar flow by 2% for the sphere and 1% for the prolate spheroid. The oblate capsule had the same response time in all flows. Matching experimental measurements of the time response with this numerical model is another way to infer capsule stiffness.

The mean local strain energy stored in the capsule at steady-state was calculated by evaluating the strain energy on each capsule mesh element, and then taking an element-size-weighted mean of the local strain energies. The formula used for this calculation is,

$$\langle W\rangle=\frac{1}{A_c Eh}\sum_i\left(\frac{Eh}{3}\left(\lambda_{1i}^2+\lambda_{2i}^2+1/\left(\lambda_{1i}^2\lambda_{2i}^2\right)-3\right)A_i\right), \quad (20)$$

where λ_{1i} and λ_{2i} are the principal stretch ratios on element i, A_i is the initial area of element i, and A_c is the initial surface area of the capsule. The mean strain energy is shown for both uniaxial-planar and biaxial-planar flow in Figure 11. The reported strain energies

are dimensionless, they are normalized by the membrane stiffness. For both flows, $\langle W \rangle$ increases with q to a maximum at $q = 1$, planar flow.

The deformation of spheres for $Ca = 0.01$, 0.02, and 0.04 was also modeled; these simulations were performed with the same parameters as before, with the same variation in q. Figure 12 shows D scaled by Ca for each of the different combinations of q and Ca. These results are scaled by Ca because the linear perturbation theory of Barthès-Biesel& Rallison (1981) predicts that D and Ca are proportional for small deformations of spheres. At the lower Ca of 0.01 and 0.02, D varies linearly with q, which also agrees with the predictions made by the perturbation analysis, because the steady-state shape distortion is proportional to the flow gradient matrix for small deformations. For larger Ca, the increase of D with Ca is sub-linear; nonlinear response is expected for large shape distortions. This sub-linear response is consistent with experiments on planar extensional flow (Chang & Olbricht 1993*b*) and with simulations of spherical capsules in shear flow (Pozrikidis 1995, Eggleton & Popel 1998). The relative change in surface area is shown for varying Ca in Figure 13; this relative change in surface area is calculated as in Figure 8, but scaled by Ca^2. For a given Ca, planar and biaxial flows led to roughly the same increase in surface area; uniaxial flow led to less surface area increase.

The relative response time, τ/Ca, is shown in Figure 14; this was calculated in the same manner as for Figure 10. While τ is slightly non-monotonic with q for $Ca = 0.04$, it varies linearly with q for lower Ca. In Figure 15, the mean strain energy $\langle W \rangle$ is shown scaled by Ca^2; this scaling was chosen because spring energy is proportional to the square of the change in characteristic length, and, for small deformation, shape distortion is proportional to Ca. For each q, the strain energy is very close to proportional to Ca^2, indicating that defining the characteristic strain rate, $\dot{\varepsilon}$ as the 2-norm of the symmetric part of the flow gradient matrix, **E**, is not just convenient, it is physically relevant.

The parameters D, τ, $\langle W \rangle$ and change in surface area vary with q similarly, regardless of Ca. By appropriately orienting the coordinate system, the results found here apply to each capsule in any irrotational flow for the capillary numbers modeled here, 0.01, 0.02, and 0.04, because any irrotational linear flow can be reduced to a superposition of planar and uniaxial or planar and biaxial extensional flow when considering capsule deformation physics.

Moreover, because rigid body rotation has a negligible effect on the deformation of spheres at low capillary numbers (Barthès-Biesel & Rallison 1981), these results apply to the spherical capsule in any linear flow at the capillary numbers shown here, not just irrotational flows. Characterizing flow by $\dot{\varepsilon}$ and q makes study of capsules in general irrotational flows more economical. In focusing on irrotational flow here, the effects of extension and vorticity on capsules are decoupled. Chang & Olbricht (1993*a*) studied spherical capsules in shear and irrotational planar extensional flow, and found that the capsules in the irrotational flow burst at a much lower capillary number. For ellipsoidal capsules, the vortical component of flow mitigates capsule deformation caused by extension. Although only irrotational flows were modeled here, the extent of the deformation of a capsule reported here is an upper-bound for a given Ca and q in vortical flow.

If the different flows were to be compared, for a given capsule, planar flow leads to more deformation (measured by deformation factor and by change in surface area) and deforms the capsule into a more energetic shape than the other two cases; by these metrics, biaxial flows are the next most intense. Any comparison of the effects of different types of flows on capsules is ambiguous without a consistent metric of the intensity of the flow. For example, in (Diaz et al. 2000), capsule deformation in uniaxial extensional flow was compared with results for a capsule in simple shear flow in (Ramanujan & Pozrikidis 1998); a simple shear

flow with one Ca and a uniaxial extensional flow with a Ca less than half that of the shear flow led to the same deformation, that is, in this comparison, simple shear flow is more than half as weak as a uniaxial extensional flow. The uniaxial extensional flow was defined as, $\dot{\varepsilon}(x, -y/2, -z/2)$, the same as equation (6) here. However, the simple shear flow was formulated as $(ky, 0, 0)$ with k being the shear rate used in defining the Ca; the irrotational part of this flow field is $k/2(x, -y, 0)$, so k is $\dot{\varepsilon}/2$ using the $\dot{\varepsilon}$ defined in equation (7) here. When the Ca from (Ramanujan & Pozrikidis 1998) is rescaled, capsule deformation in simple shear is more similar to uniaxial extensional flow in (Barthès-Biesel et al. 2002).

Experiments and simulations of capsule deformation due to flow are performed in several kinds of flow fields, most notably shear, planar extensional, and uniaxial extensional, so making consistent comparisons across these different kinds of flow fields is necessary to synthesize the knowledge from these studies. The maximum principal strain rate meets this need as a parsimonious and consistent measure of flow intensity.

For different flow fields acting on a single capsule at a single Ca, the deformation factor D, response time τ, mean strain energy, and change in surface area vary by factors in the range of 1.6–2.5. The deformation factor, D is important in understanding the properties of capsules and cells: measurements of D can be used to determine the stiffness of capsules in experiments (Chang & Olbricht 1993*b*). The change in surface area and mean strain energy are useful in predicting the behavior of capsules and cells. Surface area is proportional to molecular transport across a membrane. Strain energy is useful for determining when capsules would rupture. If, say, a spherical capsule were to rupture under uniaxial extensional flow at one capillary number, it would rupture under a planar extensional flow at a lower capillary number.

This description of irrotational linear flow in terms of $\dot{\varepsilon}$ and q is also applicable to drops, bubbles, and vesicles. Capsules and drops can have qualitatively similar physical responses to flow. For example, capsules under high shear rate flow can deform into cusped shapes, which let them resist hydrodynamic forces (Dodson & Dimitrakopoulos 2008); these shapes have also been observed in drops. Bentley & Leal (1986) studied drops in different flow fields with different amounts of rotation. They reported that a drop in an irrotational flow would deform more and burst at a lower strain rate than one in a flow with rotation. However, they did not hold $\dot{\varepsilon}$ constant as they added vorticity to the flow; $\dot{\varepsilon}$ was doubled for irrotational flows compared to simple shear flows. Just as for spherical capsules, if the drop has undergone little deformation, the effect of vorticity on it is small compared to the contribution from the irrotational straining part of the flow, and so drops, in general, can be characterized by placing them in irrotational flow fields with different $\dot{\varepsilon}$ and q.

Any irrotational linear flow can be reduced to a superposition of planar and uniaxial or planar and biaxial extensional flow when considering capsule deformation physics. This is not to say that the physics of capsules in linear flows are plainly additive; however, if the principal strain rates of a flow are known, the physics of a capsule in that flow can be estimated based on the physics of the capsule in the base cases (planar, uniaxial, and biaxial flows). Capsule responses to irrotational linear flows are bounded by their responses in the base case flows.

5. Conclusion

The effect of irrotational linear flow on elastic capsules was shown to depend on two variables. The characteristic strain rate, $\dot{\varepsilon}$, is the maximum principal strain rate of the flow gradient matrix. The other variable, q, is defined here as the difference in the lesser two principal strain rates, scaled by $\dot{\varepsilon}$; this is 0 for axisymmetric flows and 1 for two-dimensional imposed flows. Irrotational linear flows acting on capsules are reduced to

superpositions of uniaxial extensional flow and planar extensional flow or of biaxial extensional flow and planar extensional flow. This reduction should also be appropriate for drops and bubbles in irrotational linear flow.

Non-spherical deformable capsules align with the principal directions of an irrotational flow; this was shown here. The long direction of the capsule aligned with the direction of the greatest extension in the flow, and the short direction of the capsule aligned with the direction of the most compression. This agrees with Jeffery's (1922) predictions for rigid ellipsoids. Knowing that ellipsoidal capsules will align with flow makes it sensible to study deformation of ellipsoidal capsules already aligned with the flow, rather than in arbitrary orientation.

The physics of capsules in linear combinations of uniaxial, biaxial, and planar extensional flow was modeled using the immersed boundary method, and the response time and steady-state deformation factor, mean membrane strain energy, and surface area were calculated. This was done for three capsules: a sphere, a prolate spheroid, and an oblate spheroid, in flows with capillary numbers of 0.01, 0.02, and 0.04. We believe that this is the first computational study of elastic capsules in biaxial flows in particular, and of capsules in superpositions of planar and axisymmetric linear flows. For the same characteristic strain rate (according to the definition used here), planar flows led to the most deformation and stored the most energy in the capsule. The deformation, D, varied linearly with q; the other parameters calculated here vary nonlinearly but monotonically with q.

Of course, it is simplistic to assume that the response of a capsule to two different kinds of flow, but at the same strain rate, would be the same. The results here illustrate this: important effects of deformation, the shape, strain energy, and time-response, can vary by factors in the range of 1.6–2.5. These results give the response of spheres and ellipsoidal capsules to irrotational linear flows, but, more importantly, they give insight regarding how to compare the behavior of capsules in different kinds of flow fields; for example, an experiment on a capsule in a uniaxial extensional flow would underpredict the deformation of that capsule in a planar flow of the same strain rate. The characterization of a flow gradient matrix by $\dot{\varepsilon}$ and q is useful in comparing capsule deformation in different flows.

Acknowledgments

A.C.S. is thankful for support from the DOE GAANN and from a Graduate Research Fellowship from the National Science Foundation. C.D.E. is supported by the NIH/NIAID R01 AI 63366. Computational support for this research was provided by Pittsburgh Supercomputing Center, supported in part by the National Science Foundation through TeraGrid resources, and by the National Institutes of Health through resources provided by the National Resource for Biomedical Supercomputing (P41 RR06009), which is part of the Pittsburgh Supercomputing Center. Additional computational support was provided by the UMBC High Performance Computing Facility (HPCF). The facility is supported by the U.S. National Science Foundation through the MRI program (grant no. CNS-0821258) and the SCREMS program (grant no. DMS-0821311), with additional substantial support from the University of Maryland, Baltimore County (UMBC).

References

Bagchi P, Johnson PC, Popel AS. J Biomech Eng. 2005; 127:1070–1080. [PubMed: 16502649]

Bagchi P, Kalluri R. Phys Rev E. 2009; 80:016307.

Barthès-Biesel D. J Fluid Mech. 1980; 100(4):831–53.

Barthès-Biesel D, Chhim V. Int J Multiphase Flow. 1981; 7(5):493–505.

Barthès-Biesel D, Diaz A, Dhenin E. J Fluid Mech. 2002; 460:211–222.

Barthès-Biesel D, Rallison JM. J Fluid Mech. 1981; 113:251–267.

Barthès-Biesel D, Sgaier H. J Fluid Mech. 1985; 160:119–135.

Bentley B, Leal LG. Journal of Fluid Mechanics. 1986; 167(1):241–283.

Chang KS, Olbricht WL. a J Fluid Mech. 1993; 250:609–633.

Chang KS, Olbricht WL. b J Fluid Mech. 1993; 250:587–608.

Chorin AJ. Math Comp. 1968; 22(104):745–762.

Diaz A, Barthès-Biesel D, Pelekasis NA. Phys Fluids. 2001; 13(12):3835–3838.

Diaz A, Pelekasis NA, Barthès-Biesel D. Phys Fluids. 2000; 12(5):948–957.

Doddi SK, Bagchi P. Phys Rev E. 2009; 79(4):046318.

Dodson WR, Dimitrakopoulos P. Phys Rev Lett. 2008; 101(20):208102. [PubMed: 19113382]

Dodson WR, Dimitrakopoulos P. J Fluid Mech. 2009; 641:263–296.

Eggleton CD, Popel AS. Phys Fluids. 1998; 10(8):1834–1845.

Gupta NR, Nadim A, Haj-Hariri Hz, Borhan A. J of Colloid Interf Sci. 2009; 252:236–248.

Jeffery GB. Proc R Soc A. 1922; 102(715):161–179.

Kraus M, Wintz W, Seifert U, Lipowsky R. Phys Rev Lett. 1996; 77(17):3685–3688. [PubMed: 10062282]

Oden, JT. Finite Elements of Nonlinear Continua. McGraw Hill; New York: 1972.

Pappu V, Doddi SK, Bagchi P. J Theor Biol. 2008; 254(2):483–498. [PubMed: 18597788]

Peskin CS. J Comput Phys. 1977; 25(3):220–252.

Peskin CS, Printz BF. J Comput Phys. 1993; 105:33–46.

Pozrikidis C. J Fluid Mech. 1995; 297:123–152.

Ramanujan S, Pozrikidis C. J Fluid Mech. 1998; 361:117–143.

Rehage H, Husmann M, Walter A. Rheol Acta. 2002; 41(4):292–306.

Shin SJ, Sung HJ. Phys Rev E. 2011; 83(4):046321.

Song C, Shin SJ, Sung HJ, Chang KS. J Fluids Struct. 2011; 27(3):438–455.

Sui Y, Low HT, Chew YT, Roy P. Phys Rev E. 2008; 77(1):16310.

Taylor GI. Proc R Soc A. 1923; 103(720):58–61.

Walter A, Rehage H, Leonhard H. Colloids and Surfaces A: Physicochem and Eng Aspects. 2001; 183:123–132.

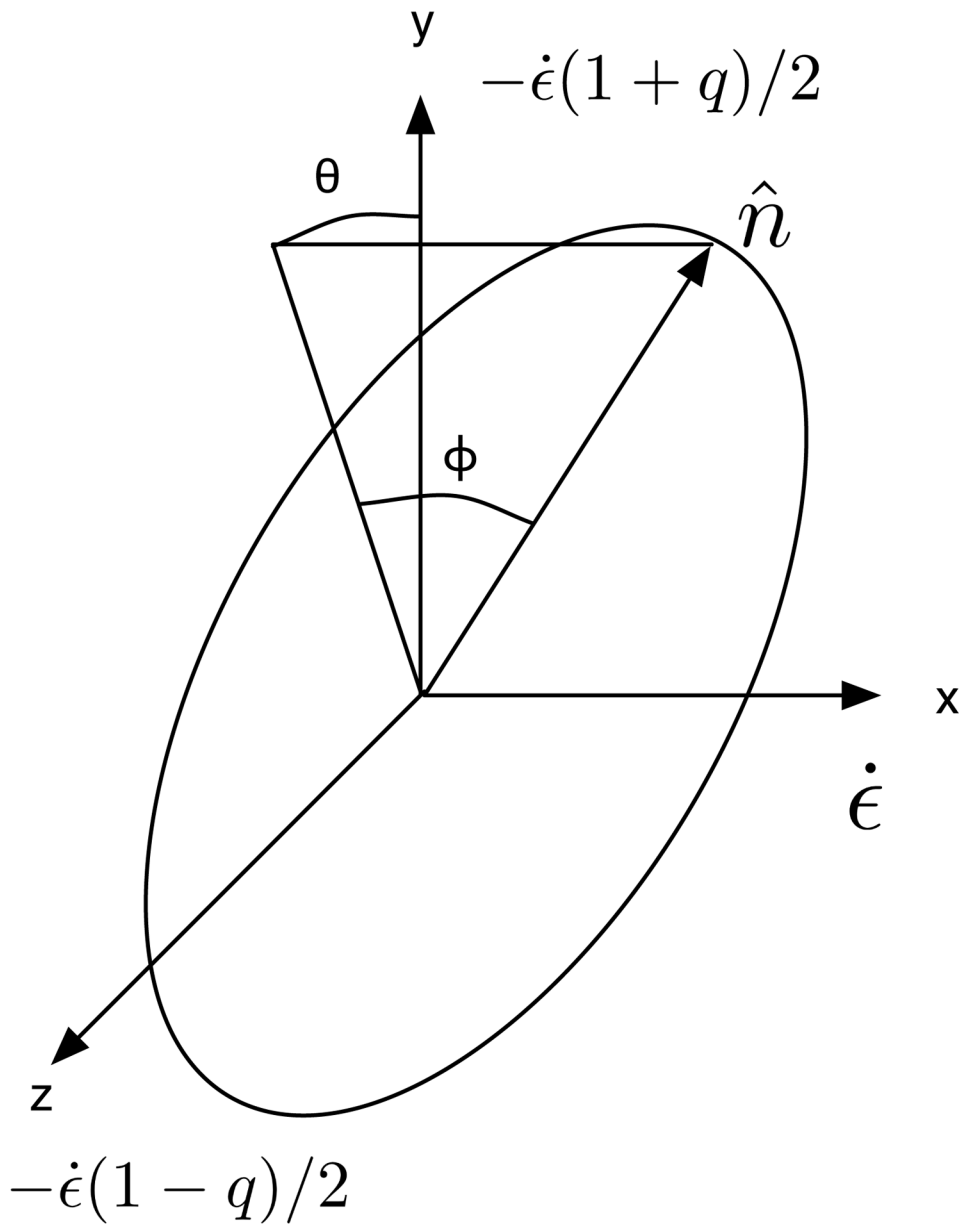

Figure 1.
Schematic of orientation of capsule in a combination of uniaxial and planar extensional flows.

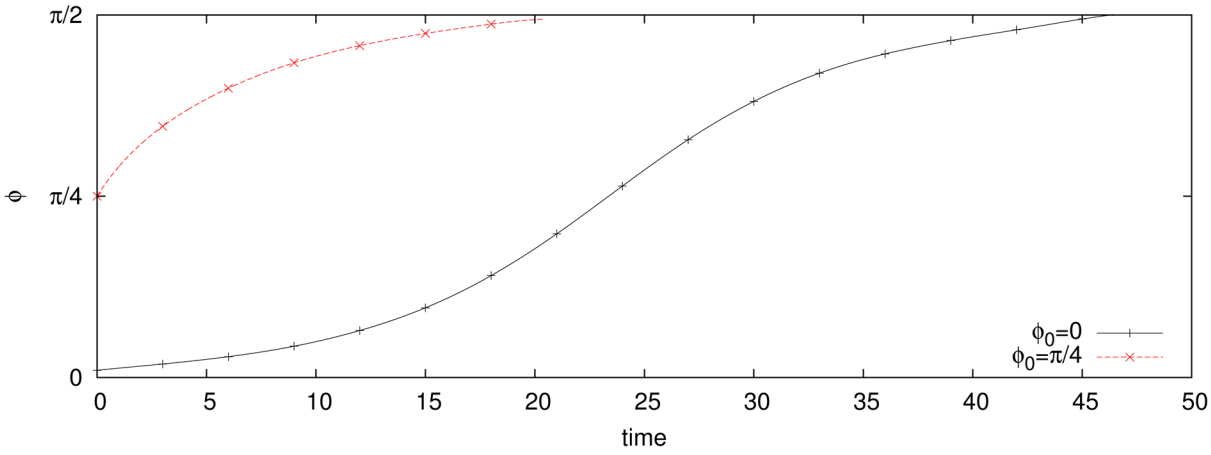

Figure 2.
The angle of elevation from the $y-z$ plane, φ, of a prolate capsule under a uniaixial extensional flow.

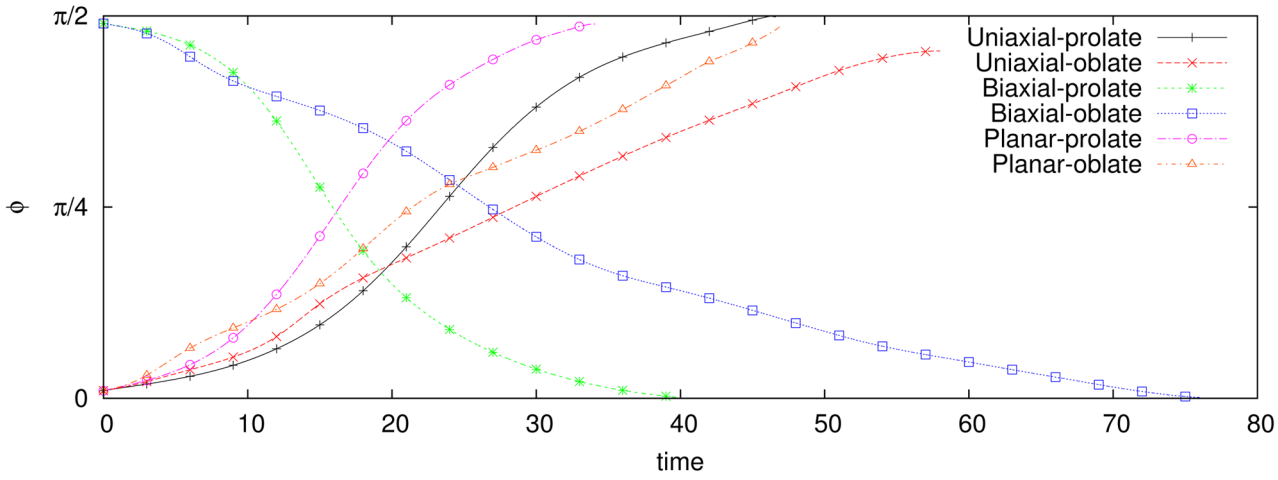

Figure 3.
Orientation of prolate and oblate capsules in uniaxial, biaxial, and planar flows.

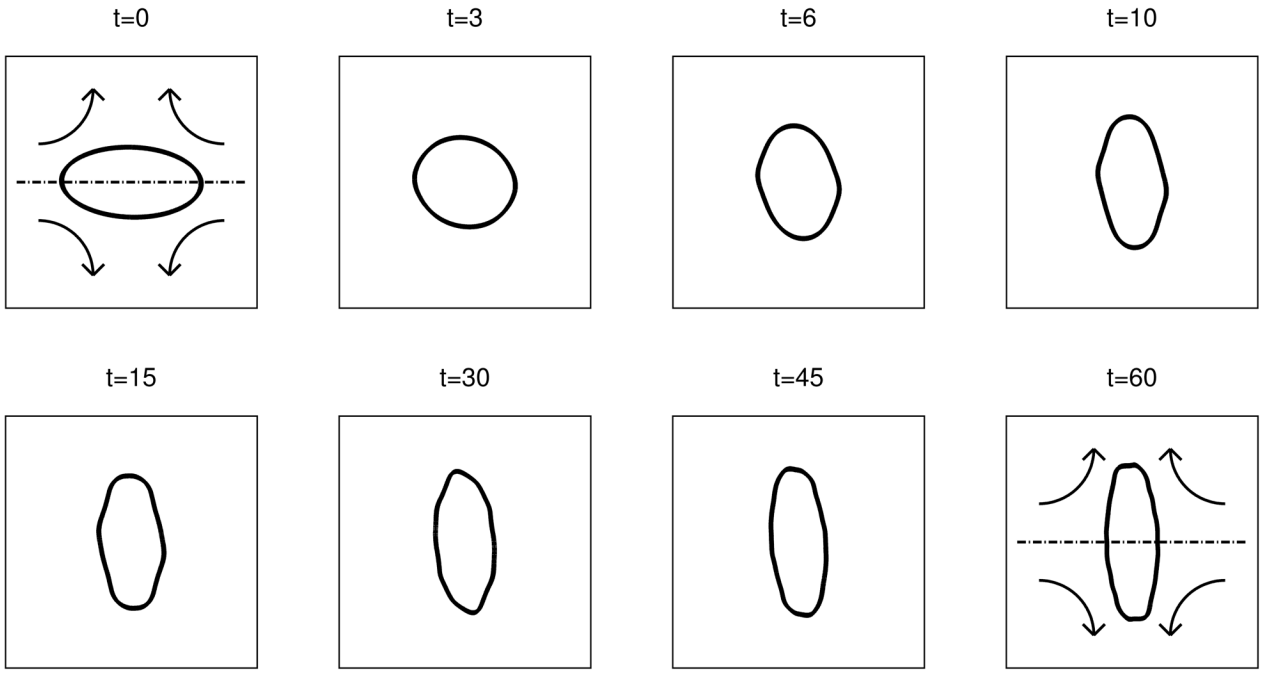

Figure 4.
Profile of an oblate spheroid capsule under biaxial extensional flow. The direction of the flow is indicated in the first and last frames, with the dashed line indicating the axis of symmetry for the flow.

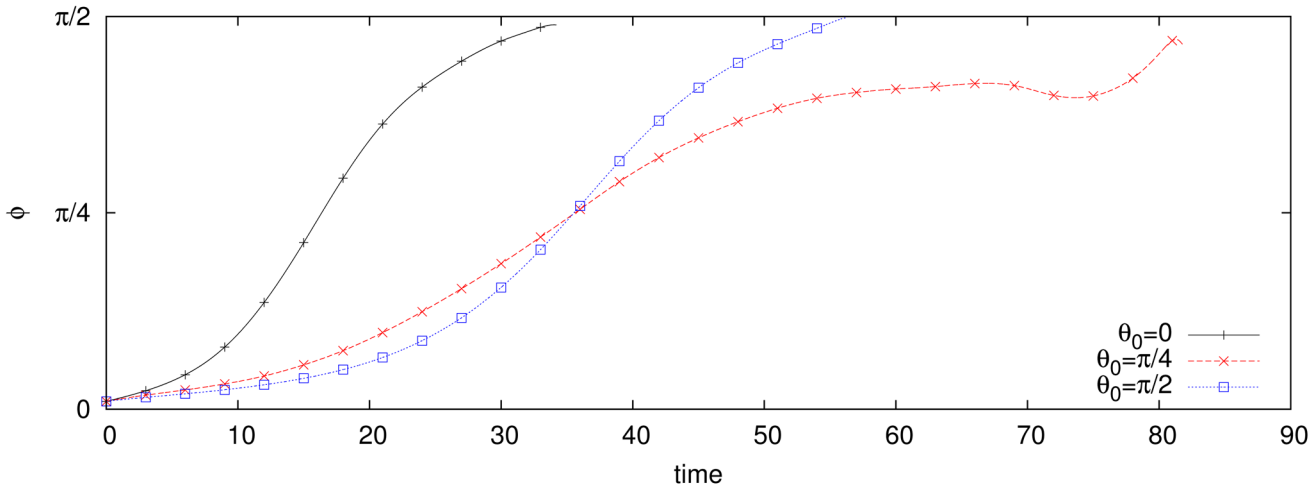

Figure 5.
Alignment of a prolate spheroid in planar extensional flow.

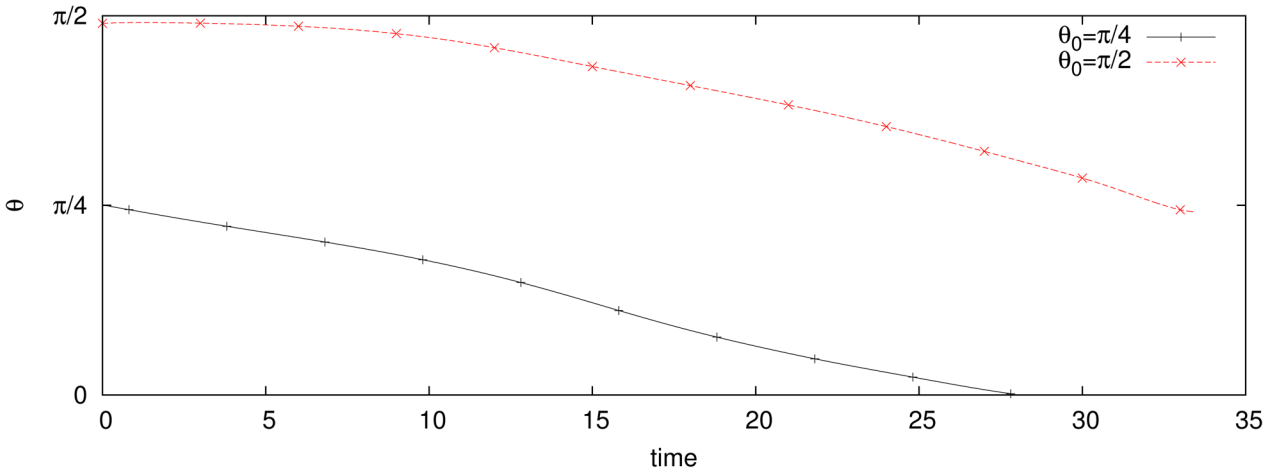

Figure 6.
The azimuthal angle, θ, of an oblate capsule in a planar extensional flow, with different initial θ.

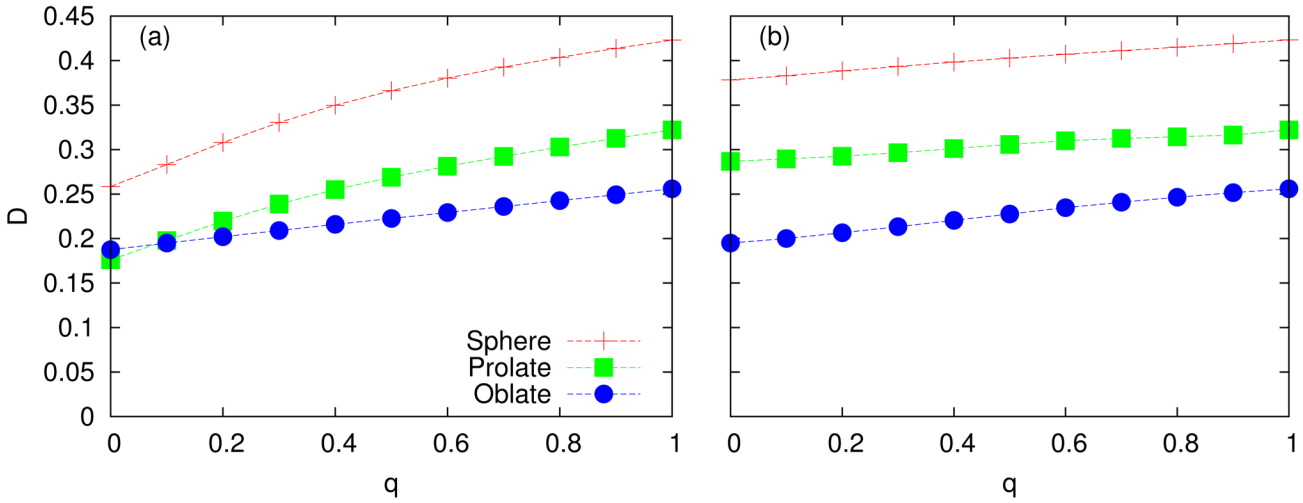

Figure 7.
The steady-state deformation, measured as *D*, is shown as a function of *q*, for both the (a) uniaxial-planar and the (b) biaxial-planar extensional cases.

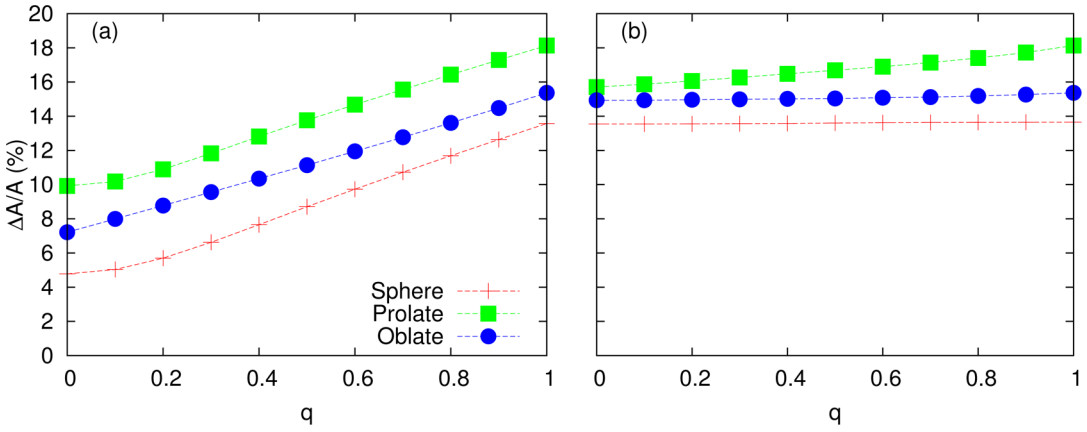

Figure 8.
The increase in the surface area of the capsule due to imposed flow is shown as a function of *q*, for both the (a) uniaxial-planar and the (b) biaxial-planar extensional cases.

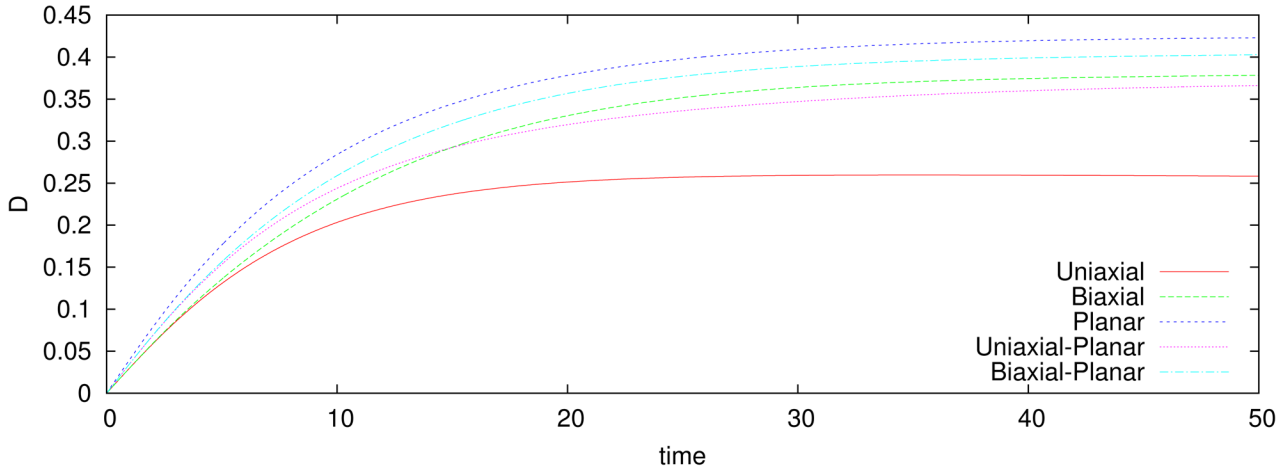

Figure 9.
The time evolution of the deformation of spherical capsules. The flows marked Uniaxial-Planar and Biaxial-Planar are given by equations (4) and (5), respectively, for $q = 0.5$.

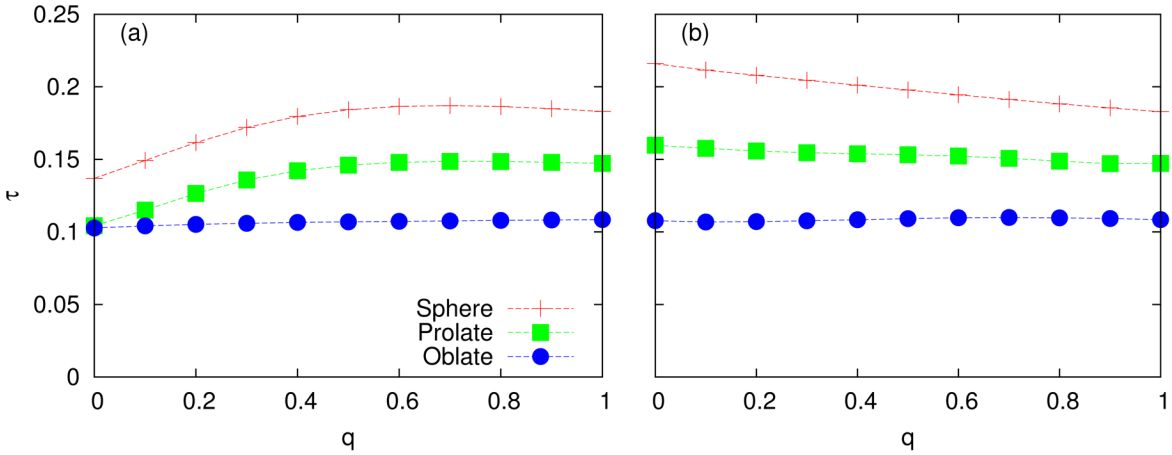

Figure 10.
Response time is shown for as a function of *q*, for both the (a) uniaxial-planar and the (b) biaxial-planar extensional cases.

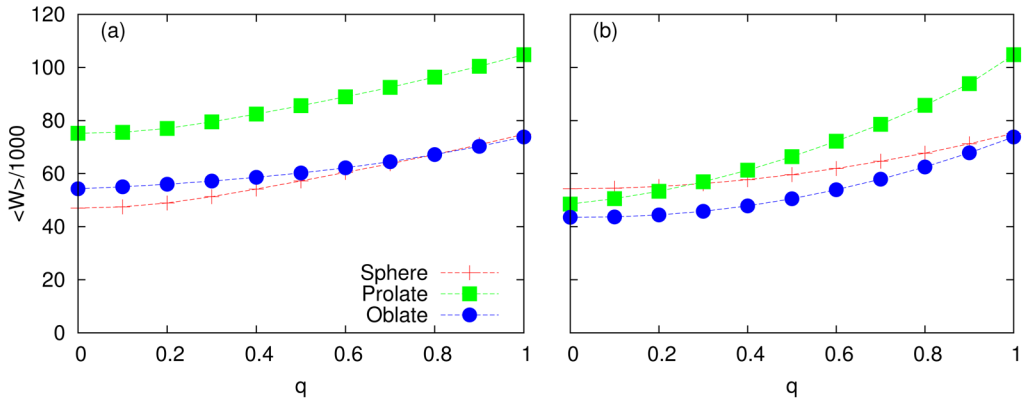

Figure 11.
The mean strain energy (nondimensional) is shown as a function of *q*, for both the (a) uniaxial-planar and the (b) biaxial-planar extensional cases.

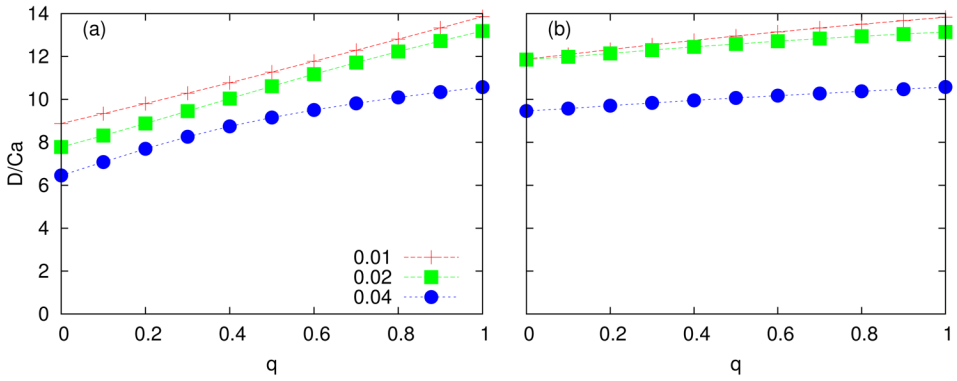

Figure 12.
The steady-state deformation, measured as *D*, is shown as a function of *q*, for both the (a) uniaxial-planar and the (b) biaxial-planar extensional cases.

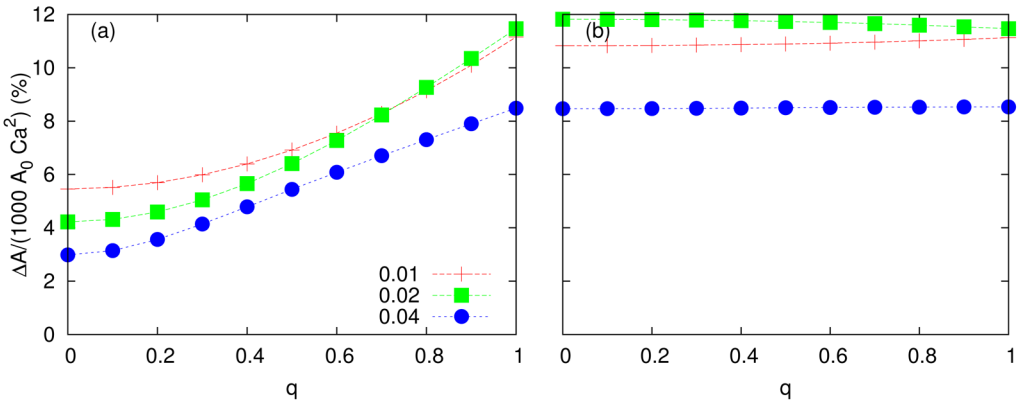

Figure 13.
The increase in the surface area of the capsule due to imposed flow is shown as a function of *q*, for both the (a) uniaxial-planar and the (b) biaxial-planar extensional cases.

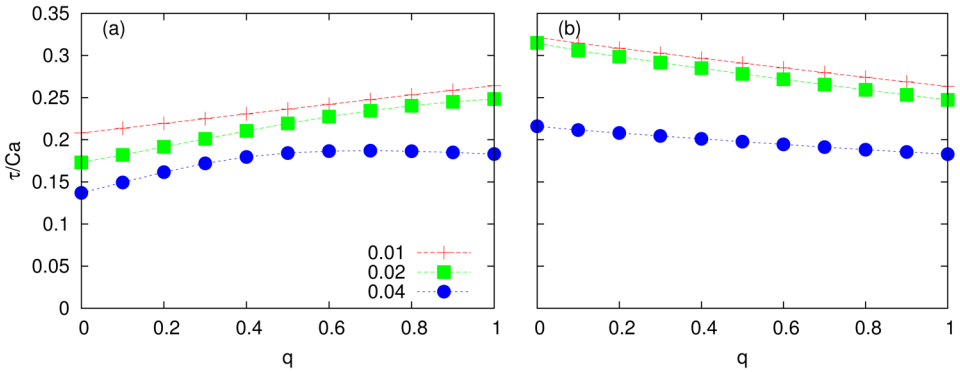

Figure 14.
Response time is shown for as a function of *q*, for both the (a) uniaxial-planar and the (b) biaxial-planar extensional cases.

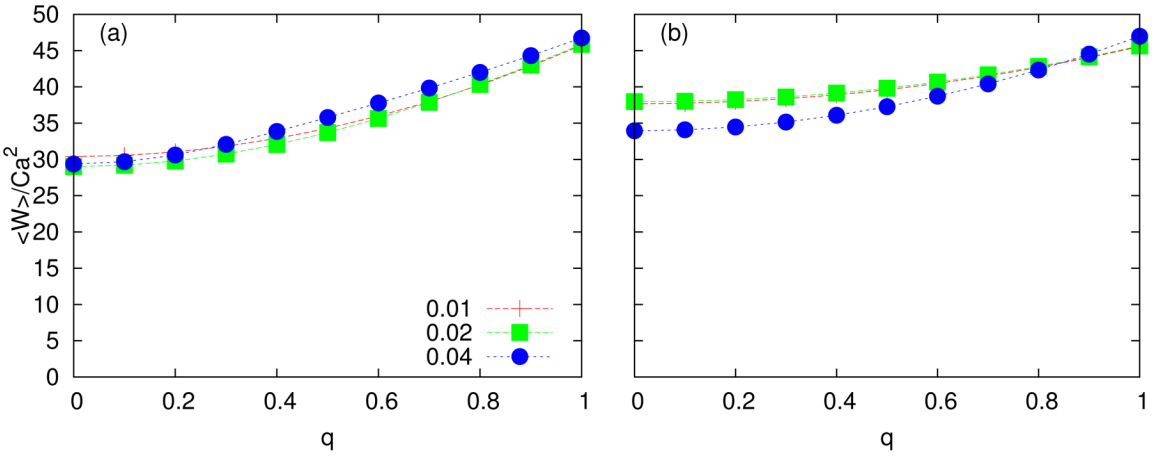

Figure 15.
The mean strain energy (nondimensional) is shown as a function of *q*, for both the (a) uniaxial-planar and the (b) biaxial-planar extensional cases.